Accepted Manuscript

Quarterly Journal of Engineering Geology and Hydrogeology

Forecast climate change impact on pore-water pressure regimes for the design and assessment of clay earthworks

Wengui Huang, Fleur A. Loveridge, Kevin M. Briggs, Joel A. Smethurst, Nader Saffari & Fiona Thomson

DOI: https://doi.org/10.1144/qjegh2023-015

To access the most recent version of this article, please click the DOI URL in the line above. When citing this article please include the above DOI.

This article is part of the Climate change and resilience in Engineering Geology and Hydrogeology collection available at: https://www.lyellcollection.org/topic/collections/Climate-change-and-resilience-in-engineering-geology-and-hydrogeology

Received 24 February 2023
Revised 28 July 2023
Accepted 25 September 2023

Forecast climate change impact on pore-water pressure regimes for the design and assessment of clay earthworks

Wengui Huang[1], Fleur A. Loveridge[2*], Kevin M. Briggs[3], Joel A. Smethurst[4], Nader Saffari[5], Fiona Thomson[6]

1. School of Computing, Engineering & Digital Technologies, Teesside University, Middlesbrough, UK
2. School of Civil Engineering, University of Leeds, Leeds, UK
3. Department of Architecture and Civil Engineering, University of Bath, Bath, UK
4. School of Engineering, University of Southampton, Southampton, UK
5. Engineering (Earth Structures & Geotechnical), Transport for London, London, UK
6. Engineering & Asset Strategy, Transport for London, London, UK

ORCID: WH, 0000-0002-4177-8156; FAL, 0000-0002-6688-6305; KMB, 0000-0003-1738-9692

*Correspondence: F.A.Loveridge@leeds.ac.uk

Abstract: Understanding and mitigating the impact of climate change on the built environment is becoming increasingly important worldwide. Earthworks (embankments and cuttings) supporting road and rail transportation networks often have direct contact with the atmosphere and are therefore influenced by extreme weather events and seasonal weather patterns. Atmospheric wetting and drying alters pore-water pressures (PWP) within earthworks, potentially contributing to the deformation and failure of earthwork slopes. Consequently, it is essential to understand the influence of climate change on PWPs within earthwork slopes, to inform strategies for their design, assessment and maintenance. Extensive one-dimensional seepage analyses were carried out for typical railway embankments in the London area. The analyses showed that forecast hotter, drier summers will increase the water storage capacity of earthworks. This will lead to increased net infiltration in the winter months due to both a

forecast increase in rainfall, and a longer time being required to saturate the soil pores and bring the water table back to the slope surface. Hence, despite the forecast increase in winter rainfall, this will not lead to higher design PWP regimes. The analyses were conducted for the London area, but the methodology and conceptual framework can be readily adapted for other locations.

Keywords: climate change; cutting; embankment; pore-water pressure; slope stability

Acronyms

1D	One-dimensional
2D	Two-dimensional
AET	Actual evapotranspiration
CMIP	Coupled Model Intercomparison Project
CNI	Cumulative net infiltration
HP model	Higher permeability model
Hr	Hydrostatic ratio
LCI	Land climate interaction
LP model	Lower permeability model
NI	Net infiltration
PET	Potential evapotranspiration
PPE	Perturbed parameter ensemble
PWP	Pore-water pressure
RCP	Representative contraction pathway
SMD	Soil moisture deficit
SVAT	Soil-Vegetation-Atmosphere-Transfer
UKCP18	United Kingdom Climate Projections 2018

UKCP09	United Kingdom Climate Projections 2009
UKCIP02	United Kingdom Climate Impacts Programme 2002
WSC	Water storage capacity

1. Introduction

Understanding and mitigating the impact of climate change is becoming an increasing challenge worldwide. All infrastructure can be affected by climate change, for example, predicted increases in the frequency of extreme temperatures and severe flooding will lead to damage to transport networks (CCC, 2021; Dodman et al. 2022). Geotechnical structures are specifically vulnerable to climate effects as they often have direct contact with the atmosphere (Tarantino et al. 2016). Climate change effects could be coupled with increasing human disturbance and activities, which further drives risk (Ozturk et al. 2022; Zhang et al. 2013, 2022). The UK independent assessment of climate risk rates the potential adverse impacts from slope and embankment failure on transport networks as its highest urgency score (CCC, 2021). This risk is compounded by the age (up to 170 years) of many transport embankments and cuttings in the UK (Spink, 2020), which are known to be deteriorating (e.g., Briggs et al. 2017; Rouainia et al. 2020; Postill et al. 2021). For example, data from Network Rail shows annual failure rates of 0.06% and 0.27% for soil embankments and cuttings respectively between April 2019 and March 2020. These annual rates are respectively three and two times the average rates recorded for the seventeen years from 2003 to 2020 (Mair, 2021).

In the UK, there is no discernible trend in annual precipitation but a clear trend for annual temperature, in both the historical weather record (Lee, 2020) and future climate projections (Jenkins et al. 2009; Lowe et al. 2018). The increase in temperature is projected to have an impact on seasonality, with summer becoming hotter and drier, and winter warmer and wetter

(Dixon and Brook, 2007; Jenkins et al. 2009; Lowe et al. 2018). These changes are expected to lead to adverse impacts for both natural slopes (e.g. Moore et al, 2010), and earthworks (e.g. Rouainia et al, 2020). One way in which climate change will influence earthwork behaviour is by altering pore-water pressure (PWP) regimes within earthwork slopes. PWPs directly affect the effective stresses governing soil strength and volume change. This influences the stability (ultimate limit state) and deformation (serviceability limit state) of earthworks. PWPs are influenced by the infiltration and removal of water at or near to the slope surface due to rainfall and evapotranspiration respectively (e.g., Zhang et al. 2004; Lee et al. 2009; Smethurst et al. 2006, 2012; Briggs et al. 2013, 2016). Climate change could alter the magnitude, duration and timing of rainfall infiltration and evapotranspiration. Consequently, it is essential to understand the effect of these changes on PWP development. If climate change causes higher PWPs, it would mean that many existing slopes which were designed using PWP guidelines based on the past climate may not be safe in the future climate. Furthermore, PWP guidelines (e.g., LUL, 2009) would need to be updated to take into account the effect of climate change for the design of new slopes and the adaption and remediation of existing slopes. Alternatively, if greater climate-induced drying reduces future PWPs then there is the potential for a less conservative approach in the future.

The aim of this study is to investigate the effect of forecast climate change on pore-water pressure regimes within transport infrastructure earthworks in the south east of England. This study first reviews recent approaches to the assessment of climate impacts on geo-structures (Section 2). Appropriate and up to date climate data is then selected and prepared using the UKCP18 future scenarios (Section 3). To enable a full consideration of climate uncertainty and investigate the effects of soil permeability and vegetation types, an efficient modelling strategy is adopted, and this is explained in Section 4. The key indicators used to interpret the

simulations are introduced in Section 5, and the results showing the impact of climate change on future water balance and PWP's are given in Section 6.

2. Climate Impacts Assessment Approach

Coe and Godt (2012) summarised research on the effect of climate change on geo-structures into three categories: monitoring approach, retrospective approach and prospective approach. The monitoring approach requires long-term monitoring, which is essential but can be time-consuming and costly. Both the monitoring and retrospective approaches implicitly assume that the observations in the past can be extrapolated to the future, which may not be valid in the context of climate change (Dijkstra and Dixon, 2010; Tang et al. 2018). There is increasing capability in forecasting of future climate and the numerical modelling of geo-structures making it an attractive approach that complements long-term monitoring. Table 1 provides an extensive (but not exhaustive) summary of work using this approach. Research has been carried out to investigate the effects of climate change on various geo-structures including natural slopes, transport embankments and cuttings at various locations. It should be noted that climate data is site specific, and therefore conclusions for a particular site and geological context may not necessarily be generalized to other locations (Vardon, 2015; Gariano and Guzzetti, 2016; Tang et al. 2018; Fowler et al. 2021). In addition, the ability to forecast future climate has increased in recent decades. A good example are the climate projections for the UK which have developed from CCIRG91 (1991), through UKCIP02 (Hulme et al., 2002) and UKCP09 (Jones et al. 2009) to the current UKCP18 (Murphy et al. 2018), underpinned by improved climate models of higher resolution. However, there are still various uncertainties associated with future climate modelling (Palin et al. 2021): (a) uncertainty in the future carbon emission scenarios; (b) modelling uncertainty, arising from our incomplete knowledge which limits our ability to model the climate system; (c) natural climate variability; and (d) aleatory (irreducible)

uncertainty, arising from intrinsic statistical variations of the system being modelled. The uncertainties are often captured through multiple climate models for future projections, as shown in Table 1.

Most of the existing studies shown in Table 1 used two-dimensional (2D) coupled seepage-stability analysis. This approach is widely viewed as the gold standard for analyses of individual sites involving unsaturated geomaterials and a climate boundary. However, it is computationally expensive in this context, where many scenarios must be considered to account for uncertainty, or the long time periods over which computation is required to capture decades of predicted changes. Therefore, simplifications are often made, e.g. by investigating only extreme rainfall events (Vahedifard et al. 2017, Robinson et al. 2017) or only considering a limited number of climate models over relatively short time periods (Rouainia et al. 2020; Guo, 2021). However, Lieber et al. (2022) highlighted that using projected climate for a snapshot of time could lead to overconservative design. Instead, using long-term climate data (both historical and projected) could give a more reasonable design solution. Another simplification is not to test the effects of soil permeability and vegetation types (Pk et al., 2021; Guo, 2021), but this misses important controls on both infiltration and evapotranspiration which ultimately affect PWPs.

In this study, since the research objective is to investigate the effect of climate change, it is argued that more comprehensive consideration should be given to the climate data at the cost of using a simple yet computationally efficient 1D soil model. Bussière et al. (2007) showed that that 1D seepage analysis can provide a good estimate of the hydrological response of the central part of a landfill cover system. Meanwhile, Briggs et al. (2013) also demonstrated that a 1D seepage analysis closely approximates the mid-slope condition within a 2D analysis. A

similar approach is also successfully adopted by Lieber et al. (2022) to investigate the effect of climate change on the performance of a tailings cover.

The details of the 1D hydrological model used in this study are described in Section 4. Because of the high computational efficiency of the 1D model, a wide breadth of scenarios of climate projections from UKCP18 (described in Section 3) can be fully adopted in the finite element seepage analysis. In addition, the effects of soil permeability and vegetation types are investigated through a series of parametric studies (described in Section 4) in the context of climate change.

3. Climate data

3.1. Introduction to UK Climate Projections 2018 (UKCP18)

The climate data used in this study were taken from UK Climate Projections 2018 (UKCP18), which is the latest national set of climate projections for the UK (Murphy et al. 2018). UKCP18 uses one of the latest versions of the Met Office United Model, HadGEM3-GC3.05 (hereafter GC3.05), and provides spatially coherent climate projections which can be conveniently used for site specific analysis to develop narratives on the impact of climate change (Murphy et al. 2018). The projections were developed through a perturbed parameter ensemble (PPE) approach, which is a way to model climate uncertainties by perturbing model parameters within expert-specified ranges (Sexton et al., 2021; Yamazaki et al., 2021). Twelve PPEs from GC3.05 were selected by UKCP18 to downscale to regional (12 km) and local (2.2 km) scales. Both regional and local projections can better resolve physiographic features (e.g., mountains, urban effects, inland water bodies) relative to the global projections. The local projections can better simulate convective rainstorm events, and were therefore used in this study.

UKCP18 local projections provide rainfall data directly and also the climate variables required to determine potential evapotranspiration (PET). Bormann (2011) provided a comprehensive review of 18 models that can be used to estimate PET, and concluded that PET models should be validated in a regional context. Despite some debate (e.g., Chun et al. 2012), the Penman-Monteith method is one of the most commonly used models for calculating PET in the UK, and has been used for site specific analyses (e.g., Postill et al. 2021; Yu et al. 2021) and to derive national sets of PET from climate observations 1969-2021 (Brown et al. 2022) and UKCP18 regional projections 1980-2080 (Robinson et al. 2021). Therefore, the Penman-Monteith method was also used in this study and PET was calculated as (Allen et al., 1998)

$$PET = \frac{0.408\Delta\,(R_n - G) + \gamma \frac{900}{T+273} u_2 (e_s - e_a)}{\Delta + \gamma(1 + 0.34 u_2)} \quad (1)$$

where Δ is the slope of the vapour pressure curve [kPa/°C]; R_n is the net solar radiation [MJ/m^2/day]; G is the surface heat flux [MJ/m^2/day]; γ is the psychrometric constant [kPa/°C]; T is the mean daily air temperature [°C]; e_s and e_a are the saturation and actual vapour pressure [kPa], respectively; and u_2 is the wind speed at 2 m height [m/s].

The climate variables from UKCP18 local projections are for three discontinuous periods 1981-2000, 2021-2040 and 2061-2080. It should be noted that the climate variables for the historical period (i.e., 1981-2000) are not the same as the historical weather record. However, they have been calibrated with historical weather records (Yamazaki et al. 2021) and therefore can be used as a baseline. There is uncertainty in future carbon emissions. UKCP18 local projections assume the highest carbon emissions scenario, RCP8.5 (Meinshausen et al. 2011). For a given carbon emission scenario, there is still uncertainty in the future climate projections. The uncertainty is captured by the 12 diverse PPEs covering a broad range of climate scenarios (Murphy et al. 2018).

3.2. Location of the site

Climate data are site specific. Initial sensitivity studies showed that much of the north and west of the UK were likely to retain hydrostatic worst-case PWP conditions, and therefore a location with greater drying was chosen to understand the nuance of future pore water pressure changes in a region subjected to greater change. This study therefore focusses on the London area, which is a region with significant drying potential (Harrison et al, 2012) and the highest density of infrastructure earthworks in the UK. The UKCP18 climate projections were taken for London Heathrow Airport. Figure 1 shows a comparison of annual average mean air temperature (T_{mean}) at 1.5 m (above the ground surface) from the historical weather record and for clarity averages of the 12 individual PPEs from UKCP18 local and regional projections. It should be noted that averages of the 12 PPEs give a low variability, but a higher variability can be observed in the individual PPEs (Huang et al. 2023) and in the historical weather record. An increasing trend of T_{mean} can be observed from the historical records. The average T_{mean} was 10.2°C for 1901-1920, 11.7°C for 2001-2020, and is projected to increase further to 14.7°C for 2061-2080 assuming carbon emissions follow RCP8.5. Figure 1 shows that UKCP18 local and regional projections give identical results for T_{mean}, but regional projections significantly over-predict annual rainfall compared to both local projections and historical records for this site (not shown). This was also a reason why this study adopted the UKCP18 local projections.

3.3. Change of climate pattern

The annual rainfall and PET derived using Eq. (1) for the UKCP18 local projections are shown in Figure 2. The magnitude of the annual rainfall and PET are comparable for 1981-2000. There is clearly an increase in PET with time, which is attributed to the increase in temperature shown in Figure 1. No clear trend is shown for annual rainfall with time, which is consistent with the observations in the historical weather record (Lee, 2020) and climate projections (Jenkins et al.

2009; Lowe et al. 2018). The annual PET is clearly above annual rainfall by 2061-2080 (Figure 2c). Comparisons of monthly averages for rainfall and PET are shown in Figure 3. In summer, which is defined as from April to September in this study, there is an increase in PET and decrease in rainfall with time. In the winter months (October to March), there is a slight increase in PET with time, but significantly greater rainfall, particularly in mid-winter (December, January and February). The change of rainfall pattern (i.e., decrease in summer and increase in winter) can also be attributed to future changes in temperature. Atmospheric water-holding capacity is expected to increase exponentially with temperature (Min et al. 2011). The projected increase of temperature is greater in summer than in winter in the southern England (Murphy et al. 2018). Consequently, more water is expected to be held in the atmosphere in summer leading to reduced rainfall, whereas the water-holding capacity is reached in winter leading to greater rainfall.

4. Finite element seepage analysis

The finite element program SEEP/W, which is part of the GeoStudio software package, was adopted in this study. Therefore, only the hydrological response of a slope due to climate change was considered. While neglecting the mechanical response to pore water pressure changes removes a direct link to stability assessment, the results can still be used to infer its effect on known mechanisms of earthwork deterioration, or as an input to non-coupled stability analysis. By ignoring water compressibility, vapor transfer and thermal effects, the governing equation for water flow in porous medium can be written as (Geo-Slope International Ltd, 2020)

$$m_v \frac{\partial u_w}{\partial t} + m_w \frac{\partial (u_a - u_w)}{\partial t} = \frac{\partial}{\partial z}\left(\frac{k_w}{\rho_w g}\frac{\partial u_w}{\partial z} + k_w\right) - S \quad (2)$$

where m_v is the compressibility coefficient of the soil structure, m_w is the slope of the soil-water retention curve (SWRC), k_w is the water permeability of the soil. Both m_w and k_w are

highly nonlinear function of matric suction ($u_a - u_w$). S is a sink term used to model the rate of water taken out of the model through actual evapotranspiration (AET).

4.1. Soil profiles and parameters

The geometry of two representative 1D soil models is shown in Figure 4. One-dimensional (1D) models can be used to calculate climate-induced changes in pore water pressure within uniform slopes (Blight, 1997; Li et al. 2005; Dijkstra & Dixon, 2010), and applied to embankments and cut slopes (Fourie et al. 1999; Gavin & Xue, 2008; Briggs et al. 2013). Therefore, 1-D models are also used in this study to investigate the impact of climate change on PWP regimes in clay earthworks, for the general case. The 1-D models represent the mid-slope of typical railway embankments (i.e. away from the slope crest and toe) on the London Underground Ltd network (Briggs et al. 2013), but do not represent the geometry of individual slopes. Each model consists of three layers, i.e., surface clay fill (1 m), clay fill (4 m) and London Clay foundation (4 m). The difference between the two models lies in the permeability of the clay fill. The saturated permeability $k_s = 5 \times 10^{-8}$ m/s for the clay fill in the first model is slightly greater than the median value of 3×10^{-8} m/s for old clay fill embankments constructed by end tipping in the 19th century (O'Brien et al., 2004). In the second model, the clay fill permeability $k_s = 5 \times 10^{-9}$ m/s is likely to be a lower bound for old clay fill embankments (O'Brien et al. 2004) and has the same order of magnitude as the in-situ London Clay (Chandler et al. 1990) and modern well compacted embankments. In both models the fill is underlain by London Clay with $k_s = 5 \times 10^{-9}$ m/s. Therefore the lower permeability model in Figure 4 could also be taken as representative of some clay highway embankments and some clay cuttings. The surface clay layer is assigned a higher permeability $k_s = 5 \times 10^{-7}$ m/s, which captures the increase in permeability at the near surface of earthworks due to weathering and desiccation cracking (Dixon et al. 2019). The desiccation crack depths reported by Yu et al. (2021) from a

long-term field monitoring of a clay fill embankment in Northumberland (UK) were generally less than 0.3m and did not exceed 1m, which justifies the use of 1m as an upper bound for the depth of the surface clay fill. As the clay fill of the first model is 10 times more permeable than the second model, the two models are hereafter referred to as the higher permeability (HP) and lower permeability (LP) model, respectively. Briggs et al. (2013) showed that clay embankments underlain by a much more permeable material (e.g., chalk or river terrace deposits) can maintain low PWP's even after long wet periods, and therefore are not considered in this study. Similarly, freer draining embankments and cuttings are not considered.

The soil properties are summarised in Table 2 and the hydrological properties illustrated in Figure 5. The soil-water retention curve (SWRC) for London Clay is based on the measurements by Croney (1977) and used by Briggs et al. (2013, 2016). The SWRC for the clay fill was assigned a lower air-entry value and shallower gradient than the in-situ London Clay, reflecting its greater specific volume and wider range of pore sizes (Loveridge et al. 2010; Briggs et al. 2013, 2016). Unsaturated permeability was estimated from the SWRC in conjunction with saturated permeability using the method by Mualem (1976). The soils were assumed to be slightly compressible with $m_v = 5 \times 10^{-5}$/kPa after Bell (1992).

4.2. Soil-Vegetation-Atmosphere-Transfer (SVAT) modelling

The Soil-Vegetation-Atmosphere-Transfer (SVAT) across the ground surface was modelled using the Land Climate Interaction (LCI) boundary condition in SEEP/W. The required input parameters of rainfall and PET versus time were obtained from the UKCP18 local projections (directly for rainfall, and indirectly for PET via Eq. (1)). AET depends on PET and water availability within the soil, and was calculated through a root water uptake model. The variation in key parameters are illustrated in Figure 6. The rate of root water uptake S, shown in Eq. (2),

is limited when the soil is very wet due to oxygen deficiency or when dry due to a lack of available water. Hence, S can be related to soil suction, and the relationship suggested by Feddes et al. (1978) was adopted, with the anaerobiosis point $\psi_{an} = 0$ kPa, limiting point $\psi_l = 100$ kPa and wilting point $\psi_w = 1500$ kPa. The root density was assumed to decrease linearly with depth (Indraratna et al. 2006; Tsiampousi et al. 2017). Two types of vegetation are considered here: grass and tree cover. It should be noted that PET is controlled by the evaporative demand of the atmosphere rather than an active physiological function of plants (Hillel, 2004). According to Biddle (1998), more than 99% of water taken up by plants is lost as transpiration, while less than 1% goes into direct growth. Therefore, it is reasonable to assume that grass and trees have the same PET, and their difference lies in the rooting depth. It should be noted that the distribution in Figure 6(b) represents the in situ plant water abstraction with depth rather than the actual root biomass (Leung et al. 2015). The root depth is set to be 0.9 m deep for grass (Briggs et al. 2013) and 3 m deep for trees (Briggs et al. 2016) based on field measurements (Biddle, 1998).

4.3. Parametric studies

The vertical height of the 1D model was 9m, and it was discretised into 90 equal elements of size 0.1m. The 1D model is very computationally efficient. Therefore, the 12 PPEs from UKCP18 local projections were all used as LCI boundary conditions in the seepage analyses with rainfall and PET input at daily resolution. The base boundary was set to be impermeable, so water could only go in or out of the top of the model. The initial water table was set to be 7m below ground surface (Figure 4) with initial PWP hydrostatic relative to the water table. The same initial condition is used for each of the three time periods 1981-2000, 2021-2040 and 2061-2080. It should be noted that the initial PWP condition can have a significant influence on model results over a short period (from days to months, e.g., Rahimi et al. 2011). A 20 year

period is modelled here, and for most of the models, the water table returns to slope surface in the first few years (an example is shown in Figure 8). Therefore, the initial PWP condition may affect the model results before it reaches full saturation, but will be minimal afterwards. The effect of climate change is evaluated by comparing the results of 2021-2040 or 2061-2080 relative to 1981-2000 (baseline), and therefore the initial PWP condition has negligible influence on the outputs of interest. It is admitted that a simple 1D model may not be as accurate as a more advanced (e.g., multidimensional coupled) model. However, since the simple model is used with both the baseline and projected climate data, the right trend in the effects of climate change is captured. In the SVAT modelling, either grass or tree cover is considered. As summarised in Table 3, a total of 144 analyses were carried out.

5. Key indicators to interpret the seepage analysis results

The key indicators used to interpret water balance and PWP conditions from the seepage analyses are explained first below, and the results are then presented in Section 6.

5.1. Cumulative net infiltration (CNI) and water storage capacity (WSC)

Net infiltration (NI) can be calculated as the balance of rainfall (P), actual evapotranspiration (AET) and runoff (RO) (e.g., Pk et al. 2021; Bashir et al. 2022),

$$NI = P - AET - RO \tag{3a}$$

and the cumulative net infiltration (CNI) can be calculated as

$$CNI = \sum P - \sum AET - \sum RO \tag{3b}$$

where $\sum$ denotes a summation with time. The value of CNI is positive to describe net infiltration and negative to describe net evapotranspiration. CNI quantifies the amount of water entering or leaving the soil. The former leads to an increase in PWP and the latter a decrease in PWP. CNI can be linked to the worst-case (i.e., maximum) PWP together with a parameter

that defines the amount of space in the soil that is able to store water. Soil moisture deficit (SMD) is commonly used to quantify the volume of water required to return the soil profile to close to a saturated state. However, the calculation of SMD is often limited to the root zone (e.g., Smethurst et al. 2012). A modified SMD is proposed here, in which the moisture deficit is evaluated within the vadose zone (down to the phreatic surface) rather than being limited to the root depth. To avoid confusion with SMD, the parameter is called water storage capacity (WSC) and can be calculated as

$$WSC = \int (\theta_s - \theta_i)\, \mathrm{d}z \tag{4}$$

where θ_s is the saturated volumetric water content, θ_i is the initial volumetric water content, and z denotes the elevation in the unsaturated zone. Both CNI and WSC should be considered relative to a point in time according to their definitions. For comparative purposes, they should be taken relative to the same time point, and the initial condition of the seepage analysis ($t = 0$) is adopted in this study. The relation between CNI, WSC and PWP can then be stated as: *when CNI equals WSC, the water table is raised to slope surface representing the maximum or worst-case PWP condition*.

The WSC relative to $t = 0$ depends on the initial PWP profile and the SWRC of the soil, and as the two models shown in Figure 4 have the same initial PWP profiles and SWRCs, the WSC of the two models is the same. The WSC of the three soil layers calculated by Eq. (4) are shown in Figure 7. The WSC for the London Clay foundation is only 7 mm, as the average suction in the London Clay is 10 kPa, which is significantly below the air-entry value and therefore the soil at initial condition is already close to full saturation. The WSC for the clay fill and surface clay fill are 149 mm and 54 mm, respectively. The total WSC of the three soil layers is therefore 210 mm.

The change of CNI with time is illustrated by an example shown in Figure 8(a). The seepage analysis was carried out for the HP model (Figure 4a) with the wettest PPE (Member 1113) and grass cover. In Figure 7 the total soil volume is assumed not to change with time, i.e., the soils are incompressible ($m_v = 0$), and therefore WSC = 0.21m. In the seepage analysis, some compressibility of the soils was considered ($m_v = 5 \times 10^{-5}$/kPa, refer to Table 2). The soil volume expands when the water is in a compressive state (i.e., PWP is positive), and WSC = 0.23m in the seepage analysis. When the CNI equals the WSC, the soil profile is completely saturated and the water table is raised to ground surface, which is the worst PWP condition possible for geotechnical stability analysis. In this situation there is no remaining water storage capacity, further rainfall infiltration is not possible and additional rainfall becomes runoff.

5.2. Hydrostatic ratio

The pore-water pressure (PWP) condition is often interpreted through a pore-water pressure profile plotted with depth (Zhang et al. 2004; Lee et al. 2009; Smethurst et al. 2006, 2012; Briggs et al. 2013). The outermost of the PWP profiles, also known as the PWP envelope, is often selected as the design condition (e.g., Lee et al. 2009). Each seepage analysis in this study (summarised in Table 3) was carried out for a 20-year period at a daily time step. The worst-case PWP (i.e., the water table reaching the slope surface) can occur for most of the models, although the frequency of occurrence is different and can be affected by soil permeability, vegetation cover and climate change.

To evaluate the frequency of worst-case PWP, each PWP profile needs to be examined. A total of 1,032,480 (> 1 million) PWP profiles were generated in the seepage analyses in this study. Interpreting each PWP profile visually and manually would not be feasible. Therefore, an index is proposed to quantify the PWP condition. To avoid confusion with the PWP ratio proposed

by Bishop and Morgenstern (1960), the index is called hydrostatic ratio (H_r). The definition of H_r is illustrated in Figure 9, and H_r is calculated as

$$H_r = \frac{A_1}{A_2} \tag{5}$$

where A_1 = the area enclosed by the PWP at a given time (where the area in which PWP's are below zero is taken as negative), A_2 = the area enclosed by the hydrostatic PWP (positive).

An example of H_r calculated using Eq. (5) is shown in Figure 8(b). Good agreement is shown between the trends of CNI in Figure 8(a) and H_r in Figure 8(b). When CNI approaches the WSC, H_r also approaches 1. The theoretical value of H_r is equal to 1 when the water table is at the ground surface. It should be noted that the maximum H_r computed from the finite element seepage analysis is often slightly less than 1 (e.g., 0.997 in Figure 8b) due to numerical error. $H_r = 0.95$ and 0.80 are indicated in Figure 8(b), and the corresponding equivalent linear PWP profiles are shown in Figure 10. It should be noted that the PWP profiles for $H_r = 0.95$ and 0.80 are not unique, but are indicators that groundwater level is approaching the slope surface. In the seepage analysis, the H_r for each day can be calculated. A "wet day" is defined here as a day on which a threshold value of H_r (e.g., 0.80, 0.95) is exceeded. It should be noted that the threshold adopted can affect the number of wet days counted, as revealed in Figure 8(b) and more clearly shown in Figure 11. There are 23 wet days for the given period if the criteria $H_r \geq 0.95$ is adopted, and 101 wet days for the criteria $H_r \geq 0.80$. By using the proposed hydrostatic ratio, the large number of PWP profiles (> 1 million) can readily be quantified, and further statistical analysis carried out. The impact of climate change on the frequency of the worst-case PWP is discussed in more detail in Section 6.2.

6. Results

All the 12 PPEs from UKCP18 local projections were used in the seepage analyses. For each PPE, seepage analyses were carried out corresponding to three periods (1981-2000, 2021-2040, or 2061-2080), two soil permeabilities (HP & LP models) and two vegetation types (grass or tree cover), as summarised in Table 3. For each period, soil permeability and vegetation type, the results can be interpreted as: 1) average of the 12 seepage analyses corresponding to the 12 PPEs; or 2) plotting the 12 sets of results as boxplots. The results related to the water balance and pore-water pressure condition are presented below using the key indicators described in Section 5.

6.1. Water balance

Analysis of the projected climate data (Figure 3) showed greater PET and less rainfall in summer and more rainfall in winter. To clearly see this seasonality, the results should be interpreted by dry/wet seasons or by months. A typical result is shown in Figure 12 for the change of monthly water balance at three time periods 1981-2000, 2021-2040 and 2061-2080 for the HP model (Figure 12a, b, c) and LP model (Figure 12d, e, f) with grass cover. In the early summer (April to June), climate change causes a significant increase in AET (due to the higher PET), negligible change in runoff, and significant increase in net evapotranspiration (due the combination of higher AET and less rainfall). In the late summer (July to September), it is interesting that the AET for 2061-2080 is the lowest (due to the limited water availability) even though the PET is the highest among the three periods. However, the change of NI is limited, as both rainfall and AET decrease. In the mid-winter (December, January and February), there is a significant increase of NI for the HP model with grass cover (Figure 12c) because of the increase in winter rainfall. However, the increase of NI for the LP model with grass cover is not obvious (Figure 12f), as the infiltration rate is governed by the soil

permeability, and the increase in rainfall intensity leads to more runoff (Figure 12e). For the other winter months (October, November, and March), there is little difference between 2061-2080 and 1981-2000 in terms of rainfall, AET, and runoff, and therefore NI is also about the same. The changes in water balance for the HP and LP models with tree cover are similar to Figure 12 and therefore not shown.

As discussed in Section 5.1 and shown in Figure 8, CNI can be linked to changes in PWP. Therefore, the impact of climate change on CNI is comprehensively investigated. Based on the characteristics of NI (Figure 12c, f) and to capture the seasonality, each year is divided into four periods: early summer (Apr., May, Jun.), late summer (Jul., Aug., Sep.), mid-winter (Dec., Jan., Feb.) and the other winter months (Oct., Nov., Mar.). For a given PPE and seepage analysis, seasonal CNI can be calculated and taken as average for the 20 years (1981-2000, 2021-2040, or 2061-2080). The seasonal CNIs from the 12 seepage analyses for each soil permeability and vegetation cover are shown in Figure 13 as boxplots. In the early summer, there is clear increase in net evapotranspiration with time for all the models. In the mid-winter, for the HP model there is clear increase in net infiltration over time (Figure 13a, b), but for the LP model the increase is not as obvious and the net infiltration is also not much different from the other winter months. The HP model has higher clay fill permeability, and therefore the net infiltration can be affected by rainfall intensity. The LP model has lower clay fill permeability, which governs the infiltration rate and the increase in rainfall intensity has little effect. The main difference between slopes with grass cover and tree cover lies in the net evapotranspiration in the late summer. For slopes with tree cover, the roots are deeper, therefore significant AET can take place even though the soil has limited water availability in late summer.

As well as the absolute magnitude of CNI, the size of the annual dry-wet cycles is also critical to slope stability, as they are directly related to shrink-swell behaviour and can drive deterioration in higher plasticity materials like London Clay (Rouainia et al. 2020; Postill et al. 2021). Clarke and Smethurst (2010) investigated the effects of climate change (using UKCIP02) on dry-wet cycles using a SMD-based soil water balance model. Their research is advanced in this study by using the more rigorous FE-based SVAT modelling and use of UKCP18. The cumulative difference of rainfall and PET (i.e., rainfall – PET) for summer (April to September) and winter (October to March) are calculated to quantify dryness and wetness, respectively. The absolute sum of these values gives a cycle size based on the climate boundary. The dry-wet cycle can also be quantified through the soil response by replacing (rainfall – PET) with seasonal CNI which takes into account the soil-vegetation-atmosphere interaction. Table 4 shows the **average** annual dry-wet cycles for both definitions, and the values shown are taken as averages for 20 years and from 12 PPEs or seepage analyses. Therefore, the values shown in Table 4 only represent the **average** scenario and do not capture the extremes (Huang et al. 2023). The values are negative for summer and positive in winter, and show clear changes in seasonality and in cycle size for the three time periods (1981-2000, 2021-2040, and 2061-2080). The climate boundary summer drying increases substantially with smaller changes in winter wetting, consistent with Figure 3. When considering the soil response, the actual drying obtained is reduced. However, it still increases in future decades, as does the soil wetting in winter. Therefore the cycle size increases between 17% and 42% depending on the soil permeability and vegetation type. The greatest impact is seen with the HP soil and trees which both facilitate deeper drying.

6.2. Frequency of the occurrence of worst-case pore-water pressure

The worst-case PWP scenario for slope stability analysis is when water table is at the slope surface. This has been quantified by use of the H_r criterion (Section 5.2) to determine the number of "wet days", defined as when the water table approaches the slope surface. It should be noted that the threshold adopted for H_r can affect the number of wet days counted, as shown in Figure 11. If there is at least one wet day in a year, that year is now also called a "wet year". The frequency of the occurrence of worst-case PWP can be examined in terms of the number of wet days per month or year and the number of wet years in a 20-year period, as discussed below. Figure 14 and Figure 15 show this information for the HP model with grass cover. Due to the space constraints, results for the other models are not shown. In general, the number of wet days decreases with the projected climate change.

The numbers of wet years in the three 20-year periods 1981-2000, 2021-2040 and 2061-2080 are shown in Figure 16. For slopes with a grass cover, the wet year frequency slightly decreases, but a wet year still occurs often enough that water table at the ground surface should be considered as the worst credible scenario. For the HP model with tree cover, AET is more effective than for the grass cover in the future periods due to a greater rooting and water abstraction depth, and the wet year frequency decreases significantly. For the LP model with tree cover, the saturated permeability of the clay fill is low ($k_s = 5 \times 10^{-9}$ m/s). The permeability is decreased further as suctions are generated by the trees, and becomes sufficiently low that it almost prevents rainfall infiltration, meaning that there are no wet years (as defined by $H_r \geq 0.80$).

6.3. A conceptual framework on the impact of climate change

Figure 17 shows a conceptual framework for the impact of climate change on the hydrological response of a slope to summer and winter weather conditions. The projected climate (Figure 3) shows that the PET will increase significantly. As a result, slopes will become drier due to greater net evapotranspiration, creating more water storage capacity. The magnitude of net evapotranspiration can be affected by vegetation type, with deeper roots allowing greater transpiration even when soil water is limited in the late summer. In winter, the change of PET is negligible, yet rainfall increases significantly. The greater water storage created in summer has two consequences. First, there is more net infiltration if the infiltration rate is governed by rainfall intensity, but net infiltration may not increase if the infiltration rate is limited by the soil permeability. Second, there is a greater soil pore space that needs to be refilled with water. Consequently, it takes a longer time to bring the water table to the slope surface, and therefore the worst-case PWP's occur less frequently.

6.4. Implications for earthworks design and management

This study was carried out for earthworks made of clay fill and/or in-situ clay with a relatively low permeability (5×10^{-8} m/s ~ 5×10^{-9} m/s) using climate projections for the London area. Although the 1D model used in this study is simple, the conceptual framework derived is useful to understand the physical impact of climate change on earthworks and the insights could be further examined with more sophisticated coupled models. The implications for earthwork design are listed below.

- The projected climate change is not expected to require higher design PWPs for analysis of deep-seated slips. A localised perched water table at shallow depth (due to weathering and desiccation cracking, etc.) is expected even with the current climate (Smethurst et al. 2006, 2012).

- Climate change will lead to increases in the magnitude of dry-wet cycles. This will drive greater shrink-swell behaviour, and may increase desiccation cracking. This also means that the rate of weather driven deterioration of soil strength is likely to increase.
- For clay slopes of low permeability, the infiltration rate is governed by the soil permeability. Therefore, the increase in rainfall intensity leads to significantly increased runoff. This may bring challenges to drainage management and potentially cause more flooding or erosional failures such as washout, in both clays and other materials.
- The projected increase of PET will have a greater impact for slopes with tree cover than grass cover, as the former has deeper roots and can transpire water even in the late summer when the availability of soil water is limited. Therefore, the vegetation management strategy of earthworks (Briggs et al. 2013b; Smethurst et al. 2015) needs to be reviewed in the context of climate change.

A comprehensive global review by Gariano and Guzzetti (2016) concluded that climate change could increase the risk of shallow landslides and debris flows, but the risk of deep-seated landslide may decrease or no significant change. This conclusion is also supported by this study.

7. Conclusions

This study investigated the impact of climate change on pore-water pressures (PWPs) for clay earthwork design. The latest national climate projections UKCP18 at the finest local scale (2.2 km) were used, based on a location in London. The highest carbon emission scenario (RCP8.5) was applied using 12 perturbed parameter ensembles (PPEs) to capture the widest possible scenarios of climate change. The key findings are summarised below.

1) The projected climate showed that there will be more potential evapotranspiration (PET) and less rainfall in summer, and more rainfall in winter. It is important to consider both precipitation and PET to forecast the effects of climate change, as the moisture deficit

created in the dry season can affect the water balance and PWP development in the wet season.

2) Due to the higher net evapotranspiration and greater water storage capacity created in summer, it takes longer time to refill the soil pores with rainwater in winter. Therefore, worst-case design PWPs for deep-seated slips are expected to occur less often, but a localised perched water table could continue to develop at shallow depth. In the future, design PWPs in clay earthworks are unlikely to be higher with climate change.
3) The magnitude of dry-wet cycles will increase in the future, by up to 42% depending on the soil and vegetation conditions. This will potentially increase the rate of strength deterioration in strain softening clay materials, increasing vulnerability to slope failures even if PWP conditions do not worsen.
4) The magnitude and spatial extent of wet-dry cycles driven by climate change will be greater where there is tree cover compared with slopes with grass cover, as the former has deeper roots and can transpire water even in the late summer when the availability of water becomes limited.
5) While slopes with lower permeability will see a smaller increase in dry-wet cycle magnitude, the increase of rainfall intensity will cause greater surface runoff, with consequences for flood risk and erosional failures.
6) Climate and climate changes projections are site specific. While the conclusions presented above are specific to one location, it is expected that the trends may be relevant for elsewhere in the UK. The modelling, interpretation methodology and conceptual framework (Figure 17) developed in this study can also be used (or adapted) for other sites.

Acknowledgement

The authors are grateful for the financial support of the Engineering and Physical Sciences Research Council (EPSRC) through the programme Grant ACHILLES (EP/R034575/1). Kevin Briggs is supported by the Royal Academy of Engineering and HS2 Ltd under the Senior Research Fellowship scheme. The authors would like to acknowledge assistance from Chris Kilsby and thank Dr David Hughes and Prof Roger Moore for reviewing and providing constructive comments to this paper.

Competing interests

The authors declare that they have no known competing financial interests or personal relationships that could have appeared to influence the work reported in this paper.

Data Statement

The UKCP18 data and historical weather data used in this study can be downloaded from https://ukclimateprojections-ui.metoffice.gov.uk/products. The derived results are freely available from the University of Leeds data repository (DOI to be confirmed).

References

Allen, R. G., Pereira, L. S., Raes, D., & Smith, M. (1998). *Crop evapotranspiration - Guidelines for computing crop water requirements - FAO Irrigation and drainage paper 56*. Food and Agriculture Organisation of the United Nations, Rome.

Bashir, R., Sahi, M. A., & Sharma, J. (2022). Using synthetic climate datasets for geotechnical and geoenvironmental design problems. *Canadian Geotechnical Journal*, 59(8), 1305-1320. https://doi.org/10.1139/cgj-2021-0408

Bell, F. G. (1992). *Engineering properties of soils and rocks* (3rd Edition). Butterworth-Heinemann Ltd.

Biddle P. G. (1998). *Tree Root Damage to Buildings*. Willowmead Publishing, Wantage, UK.

Bishop, A. W., & Morgenstern, N. (1960). Stability coefficients for earth slopes. *Géotechnique*, 10(4), 129-153. https://doi.org/10.1680/geot.1960.10.4.129

Blight, G.E., (1997). Interactions between the atmosphere and the earth. *Géotechnique*, 47(4), pp.715-767.

Booth, A. (2014). *Impacts of desiccation cracking and climate change on highway cutting hydrology*, PhD thesis, Loughborough University, UK.

Bormann, H. (2011). Sensitivity analysis of 18 different potential evapotranspiration models to observed climatic change at German climate stations. Climatic Change, 104(3-4), 729-753. https://doi.org/10.1007/s10584-010-9869-7

Briggs, K. M., Smethurst, J. A., Powrie, W., & O'Brien, A. S. (2013a). Wet winter pore pressures in railway embankments. *Proceedings of the Institution of Civil Engineers-Geotechnical Engineering*, 166(5), 451-465. https://doi.org/10.1680/geng.11.00106

Briggs, K.M., Smethurst, J.A., Powrie, W., O'Brien, A.S. and Butcher, D.J.E., (2013b). Managing the extent of tree removal from railway earthwork slopes. *Ecological engineering*, 61, pp.690-696.

Briggs, K. M., Smethurst, J. A., Powrie, W., & O'Brien, A. S. (2016). The influence of tree root water uptake on the long term hydrology of a clay fill railway embankment. *Transportation Geotechnics*, 9, 31-48. https://doi.org/10.1016/j.trgeo.2016.06.001

Briggs, K. M., Loveridge, F. A., & Glendinning, S. (2017). Failures in transport infrastructure embankments. *Engineering Geology*, 219, 107-117. https://doi.org/10.1016/j.enggeo.2016.07.016

Brown, M.J.; Robinson, E.L.; Kay, A.L.; Chapman, R.; Bell, V.A.; Blyth, E.M. (2022). Potential evapotranspiration derived from HadUK-Grid 1km gridded climate observations 1969-2021 (Hydro-PE HadUK-Grid). NERC EDS Environmental Information Data Centre. https://doi.org/10.5285/9275ab7e-6e93-42bc-8e72-59c98d409deb

Bussière, B., Aubertin, M., Mbonimpa, M., Molson, J. W., & Chapuis, R. P. (2007). Field experimental cells to evaluate the hydrogeological behaviour of oxygen barriers made of silty materials. *Canadian Geotechnical Journal*, 44(3), 245-265. https://doi.org/10.1139/t06-120

Chandler, R. J., Leroueil, S., & Trenter, N. A. (1990). Measurements of the permeability of London Clay using a self-boring permeameter. *Géotechnique*, 40(1), 113-124. https://doi.org/10.1680/geot.1990.40.1.113

Chun, K. P., Wheater, H. S., & Onof, C. (2012). Projecting and hindcasting potential evaporation for the UK between 1950 and 2099. *Climatic Change*, 113, 639-661. https://doi.org/10.1007/s10584-011-0375-3

Clarke, D., & Smethurst, J. A. (2010). Effects of climate change on cycles of wetting and drying in engineered clay slopes in England. *Quarterly Journal of Engineering Geology and Hydrogeology*, 43(4), 473-486. https://doi.org/10.1144/1470-9236/08-106

Climate Change Committee (2021). *Independent Assessment of UK Climate Risk Advice to Government for the UK's third Climate Change Risk Assessment (CCRA3)*, June 2021. Available at https://www.theccc.org.uk/wp-content/uploads/2021/07/Independent-Assessment-of-UK-Climate-Risk-Advice-to-Govt-for-CCRA3-CCC.pdf [Accessed 18th October 2022]

Climate Change Impacts Review Group (CCIRG) (1991). *The Potential Effects of Climate Change in the United Kingdom*. HMSO, London.

Coe, J. A., & Godt, J. W. (2012). Review of approaches for assessing the impact of climate change on landslide hazards, In Eberhardt, E., Froese, C., Turner, A.K., and Leroueil, S., eds., *Landslides and Engineered Slopes, Protecting Society Through Improved Understanding: Proceedings of the 11th International and 2nd North American Symposium on Landslides and Engineered Slopes*, Banff, Canada, 3-8 June, Taylor & Francis Group, London, v. 1, p. 371-377.

Collison, A., Wade, S., Griffiths, J., & Dehn, M. (2000). Modelling the impact of predicted climate change on landslide frequency and magnitude in SE England. *Engineering Geology*, 55(3), 205-218. https://doi.org/10.1016/S0013-7952(99)00121-0

Croney D. (1977). *The design and performance of road pavements*. Technical report. Her Majesty's Stationary Office.

Dixon, N., & Brook, E. (2007). Impact of predicted climate change on landslide reactivation: case study of Mam Tor, UK. *Landslides*, 4(2), 137-147. https://doi.org/10.1007/s10346-006-0071-y

Dixon, N., Crosby, C. J., Stirling, R., et al. (2019). In situ measurements of near-surface hydraulic conductivity in engineered clay slopes. *Quarterly Journal of Engineering Geology and Hydrogeology*, 52(1), 123-135. https://doi.org/10.1144/qjegh2017-059

Dijkstra, T. A., & Dixon, N. (2010). Climate change and slope stability in the UK: challenges and approaches. *Quarterly Journal of Engineering Geology and Hydrogeology*, 43 (4): 371–385. https://doi.org/10.1144/1470-9236/09-036

Dodman, D., B. Hayward, M. Pelling, V. Castan Broto, W. Chow, E. Chu, R. Dawson, L. Khirfan, T. McPhearson, A. Prakash, Y. Zheng, and G. Ziervogel, (2022): Cities, Settlements and Key Infrastructure. In: *Climate Change 2022: Impacts, Adaptation and Vulnerability*. Contribution of Working Group II to the Sixth Assessment Report of the Intergovernmental Panel on Climate Change [H.-O. Pörtner, D.C. Roberts, M. Tignor, E.S. Poloczanska, K. Mintenbeck, A. Alegría, M. Craig, S. Langsdorf, S. Löschke, V. Möller, A. Okem, B. Rama (eds.)]. Cambridge University Press, Cambridge, UK and New York, NY, USA, pp. 907–1040, doi:10.1017/9781009325844.008.

Feddes, R. A., Kowaklik, P. J., & Zaradny, H. (1978). *Simulation of field water use and crop yield*. John Wiley and Sons.

Fourie AB, Rowe D and Blight GE (1999) The effect of infiltration on the stability of the slopes of a dry ash dump. *Geotechnique* 49(1): 1–13.

Fowler, H. J., Lenderink, G., Prein, A. F. et al. (2021) Anthropogenic intensification of short-duration rainfall extremes. *Nature Reviews Earth & Environment*, 2, 107–122. https://doi.org/10.1038/s43017-020-00128-6

Gariano, S. L., & Guzzetti, F. (2016). Landslides in a changing climate. *Earth-Science Reviews*, 162, 227-252. https://doi.org/10.1016/j.earscirev.2016.08.011

Gavin, K. and Xue, J., (2008). A simple method to analyze infiltration into unsaturated soil slopes. *Computers and Geotechnics*, 35(2), pp.223-230.

Geo-Slope International Ltd. (2020). *Heat and Mass Transfer Modelling with GeoStudio*.

Guo, B. W. L. (2021). *Reuse and sustainability of flood defences*. PhD thesis, Imperial College London, London, UK.

Harrison, A. M., Plim, J., Harrison, M., Jones, L. D. & Culshaw, M.G. (2012) The relationship between shrink-swell occurrence and climate in south-east England. *Proceedings of the Geologists Association*, 123 (4), 556-575. https://doi.org/10.1016/j.pgeola.2012.05.002

Hillel, D. (2004). *Introduction to environmental soil physics*. Elsevier, Amsterdam.

Huang, W., Loveridge, F., Briggs, K., Smethurst, J. (2023). Finite element seepage modelling for earthworks in London clay with UKCP18 local projections. University of Leeds. [Dataset] doi to be provided.

Hulme, M., Jenkins, G. J., Lu, X. et al. (2002). *Climate change scenarios for the United Kingdom: the UKCIP02 scientific report*. Centre for Climate Change Research, School of Environmental Sciences, University of East Anglia, Norwich.

Indraratna, B., Fatahi, B., & Khabbaz, H. (2006). Numerical analysis of matric suction effects of tree roots. *Proceedings of the Institution of Civil Engineers-Geotechnical Engineering*, 159(2), 77-90. https://doi.org/10.1680/geng.2006.159.2.77

Jenkins, G. J., Perry, M. C., & Prior, M. J. (2009). *The climate of the UK and recent trends. UKCP09*. Met Office Hadley Centre, Exeter.

Jones, P. D., Kilsby, C. G., Harpham, C., Glenis, V., & Burton, A. (2009). *UK Climate Projections science report: Projections of future daily climate for the UK from the Weather Generator*. UK Climate Projections science report.

Kendon, E. J., Fosser, G., Murphy, J., et al. (2019). *UKCP Convection-permitting model projections: Science report*.

Lee, E. M. (2020). Statistical analysis of long-term trends in UK effective rainfall: implications for deep-seated landsliding. *Quarterly Journal of Engineering Geology and Hydrogeology*, 53(4), 587-597. https://doi.org/10.1144/qjegh2019-169

Lee, L. M., Gofar, N., & Rahardjo, H. (2009). A simple model for preliminary evaluation of rainfall-induced slope instability. *Engineering Geology*, 108(3-4), 272-285. https://doi.org/10.1016/j.enggeo.2009.06.011

Leung, A. K., Garg, A., & Ng, C. W. W. (2015). Effects of plant roots on soil-water retention and induced suction in vegetated soil. *Engineering Geology*, 193, 183-197. https://doi.org/10.1016/j.enggeo.2015.04.017

Li AG, Yue LG, Tham C and Law KT (2005) Field-monitored variations of soil moisture and matric suction in a saprolite slope. *Canadian Geotechnical Journal* 42(1): 13–26.

Lieber, E., Demers, I., Pabst, T., & Bresson, É. (2022). Simulating the effect of climate change on performance of a monolayer cover combined with an elevated water table placed on acid-generating mine tailings. *Canadian Geotechnical Journal*, 59(4), 558-568. https://doi.org/10.1139/cgj-2020-0622

Lowe, J. A., Bernie, D., Bett, P., et al. (2018). *UKCP18 science overview report*. Met Office Hadley Centre: Exeter, UK.

Loveridge, F. A., Spink, T. W., O'Brien, A. S., Briggs, K. M., & Butcher, D. (2010). The impact of climate and climate change on infrastructure slopes, with particular reference to southern England. *Quarterly Journal of Engineering Geology and Hydrogeology*, 43(4), 461-472. https://doi.org/10.1144/1470-9236/09-050

Lowe J. A., Murphy J. M., Palmer, M. D., Fung, F. (2018). *UKCP18 Science overview report.*

LUL (London Underground Ltd). (2019). *G0054B A4: Earth Structures – Guide for slope stability analysis*. London, UK: London Underground Ltd.

Mair R. (2021). *A review of earthworks management*. February 2021. Available at: https://www.networkrail.co.uk/who-we-are/our-approach-to-safety/stonehaven/ [Accessed 18 October 2022]

Meinshausen, M., Smith, S. J., Calvin, K., et al. (2011). The RCP greenhouse gas concentrations and their extensions from 1765 to 2300. *Climatic change*, 109(1), 213-241. https://doi.org/10.1007/s10584-011-0156-z

Min, S. K., Zhang, X., Zwiers, F. W., & Hegerl, G. C. (2011). Human contribution to more-intense precipitation extremes. *Nature*, 470(7334), 378-381. https://doi.org/10.1038/nature09763

Moore, R., Carey, J. M., & McInnes, R. G. (2010) Landslide behaviour and climate change: predictable consequences for the Ventnor Undercliff, Isle of Wight, *Quarterly Journal of Engineering Geology and Hydrogeology*, 43 (4): 447–460. https://doi.org/10.1144/1470-9236/08-086

Mualem, Y. (1976). A new model for predicting the hydraulic conductivity of unsaturated porous media. *Water Resources Research*, 12(3), 513-522. https://doi.org/10.1029/WR012i003p00513

Murphy, J. M., Harris, G. R., Sexton, D. M. H., et al. (2018). *UKCP18 land projections: science report.*

O'Brien A, Ellis EA and Russell D (2004) Old railway embankment fill: laboratory experiments, numerical modelling and field behaviour. In *Advances in Geotechnical Engineering: Proceedings of the Skempton Memorial Conference, Hindhead, UK* (Jardine RJ, Potts DM and Higgins KG (eds)). Thomas Telford, London, UK, vol. 2, pp. 911–921.

Ozturk, U., Bozzolan, E., Holcombe, E. A., Shukla, R., Pianosi, F., & Wagener, T. (2022). How climate change and unplanned urban sprawl bring more landslides. Nature, 608(7922), 262-265. https://doi.org/10.1038/d41586-022-02141-9

Palin, E. J., Stipanovic Oslakovic, I., Gavin, K., & Quinn, A. (2021). Implications of climate change for railway infrastructure. *Wiley Interdisciplinary Reviews: Climate Change*, 12(5), e728. https://doi.org/10.1002/wcc.728

Postill, H., Helm, P. R., Dixon, N., Glendinning, S., Smethurst, J. A., Rouainia, M., Briggs, K. M., El-Hamalawi, A., Blake, A. P. (2021). Forecasting the long-term deterioration of a cut slope in high-plasticity clay using a numerical model. *Engineering Geology*, 280, 105912. https://doi.org/10.1016/j.enggeo.2020.105912

Pk, S., Bashir, R., & Beddoe, R. (2021). Effect of climate change on earthen embankments in Southern Ontario, Canada. *Environmental Geotechnics*, 8(2), 148-169. https://doi.org/10.1680/jenge.18.00068

Rahimi, A., Rahardjo, H., & Leong, E. C. (2011). Effect of antecedent rainfall patterns on rainfall-induced slope failure. *Journal of Geotechnical and Geoenvironmental Engineering*, 137(5), 483-491. https://doi.org/10.1061/(ASCE)GT.1943-5606.0000451

Robinson, E.L.; Kay, A.L.; Brown, M.; Chapman, R.; Bell, V.A.; Blyth, E.M. (2021). Potential evapotranspiration derived from the UK Climate Projections 2018 Regional Climate Model ensemble 1980-2080 (Hydro-PE UKCP18 RCM). NERC EDS Environmental Information Data Centre. https://doi.org/10.5285/eb5d9dc4-13bb-44c7-9bf8-c5980fcf52a4

Robinson, J. D., Vahedifard, F., & AghaKouchak, A. (2017). Rainfall-triggered slope instabilities under a changing climate: comparative study using historical and projected precipitation extremes. *Canadian Geotechnical Journal*, 54(1), 117-127. https://doi.org/10.1139/cgj-2015-0602

Rouainia, M., Davies, O., O'Brien, T., & Glendinning, S. (2009). Numerical modelling of climate effects on slope stability. *Proceedings of the Institution of Civil Engineers-Engineering Sustainability*. Vol. 162, No. 2, pp. 81-89. https://doi.org/10.1680/ensu.2009.162.2.81

Rouainia, M., Helm, P., Davies, O., & Glendinning, S. (2020). Deterioration of an infrastructure cutting subjected to climate change. *Acta Geotechnica*, 15(10), 2997-3016. https://doi.org/10.1007/s11440-020-00965-1

Sexton, D. M., McSweeney, C. F., Rostron, J. W., et al. (2021). A perturbed parameter ensemble of HadGEM3-GC3. 05 coupled model projections: Part 1: Selecting the parameter combinations. *Climate Dynamics*, 56(11), 3395-3436. https://doi.org/10.1007/s00382-021-05709-9

Smethurst, J. A., Clarke, D. & Powrie, W. (2006). Seasonal changes in pore water pressure in a grass covered cut slope in London Clay. *Géotechnique*, 56(8), 523–537, http://dx.doi.org/10.1680/geot.2006.56.8.523.

Smethurst, J. A., Clarke, D., & Powrie, W. (2012). Factors controlling the seasonal variation in soil water content and pore water pressures within a lightly vegetated clay slope. *Géotechnique*, 62(5), 429-446. https://doi.org/10.1680/geot.10.P.097

Smethurst, J. A., Briggs, K. M., Powrie, W., Ridley, A., & Butcher, D. J. E. (2015). Mechanical and hydrological impacts of tree removal on a clay fill railway embankment. *Géotechnique*, 65(11), 869-882. https://doi.org/10.1680/jgeot.14.P.010

Spink, T. (2020). Strategic geotechnical asset management. *Quarterly Journal of Engineering Geology and Hydrogeology*, 53(2), 304-320. https://doi.org/10.1144/qjegh2019-014

Tang, A. M., Hughes, P. N., Dijkstra, T. A. et al. (2018). Atmosphere–vegetation–soil interactions in a climate change context; impact of changing conditions on engineered transport infrastructure slopes in Europe. *Quarterly Journal of Engineering Geology and Hydrogeology*, 51(2), 156-168. https://doi.org/10.1144/qjegh2017-103

Tarantino, A., Gallipoli, D., Jommi, C., et al. (2016). Advances in the monitoring of geo-structure subjected to climate loading. *The 3rd European Conference on Unsaturated Soils*, 12th – 14th September 2016, Paris, France. https://doi.org/10.1051/e3sconf/20160904001

Tsiampousi, A., Zdravkovic, L., & Potts, D. M. (2017). Numerical study of the effect of soil–atmosphere interaction on the stability and serviceability of cut slopes in London clay. *Canadian Geotechnical Journal*, 54(3), 405-418. https://doi.org/10.1139/cgj-2016-0319

Vahedifard, F., Tehrani, F. S., Galavi, V., Ragno, E., & AghaKouchak, A. (2017). Resilience of MSE walls with marginal backfill under a changing climate: Quantitative assessment for extreme precipitation events. *Journal of Geotechnical and Geoenvironmental Engineering*, 143(9). https://doi.org/10.1061/(ASCE)GT.1943-5606.0001743

Van Genuchten, M. T. (1980). A closed-form equation for predicting the hydraulic conductivity of unsaturated soils. *Soil Science Society of America Journal*, 44(5), 892-898.

Vardon, P. J. (2015). Climatic influence on geotechnical infrastructure: a review. *Environmental Geotechnics*, 2(3), 166-174. https://doi.org/10.1680/envgeo.13.00055

Yamazaki, K., Sexton, D. M., Rostron, J. W., et al. (2021). A perturbed parameter ensemble of HadGEM3-GC3. 05 coupled model projections: Part 2: global performance and future changes. *Climate Dynamics*, 56(11), 3437-3471. https://doi.org/10.1007/s00382-020-05608-5

Yu, Z., Eminue, O. O., Stirling, R., Davie, C., & Glendinning, S. (2021). Desiccation cracking at field scale on a vegetated infrastructure embankment. Géotechnique Letters, 11(1), 88-95. https://doi.org/10.1680/jgele.20.00108

Zhang, F., Wang, G., Kamai, T., Chen, W., Zhang, D., & Yang, J. (2013). Undrained shear behavior of loess saturated with different concentrations of sodium chloride solution. Engineering Geology, 155, 69-79. https://doi.org/10.1016/j.enggeo.2012.12.018

Zhang, F., Wang, G., & Peng, J. (2022). Initiation and mobility of recurring loess flowslides on the Heifangtai irrigated terrace in China: Insights from hydrogeological conditions and liquefaction criteria. Engineering Geology, 302, 106619. https://doi.org/10.1016/j.enggeo.2022.106619

Zhang, L. L., Fredlund, D. G., Zhang, L. M., & Tang, W. H. (2004). Numerical study of soil conditions under which matric suction can be maintained. *Canadian Geotechnical Journal*, 41(4), 569-582. https://doi.org/10.1139/t04-006

List of Figures

List of Tables

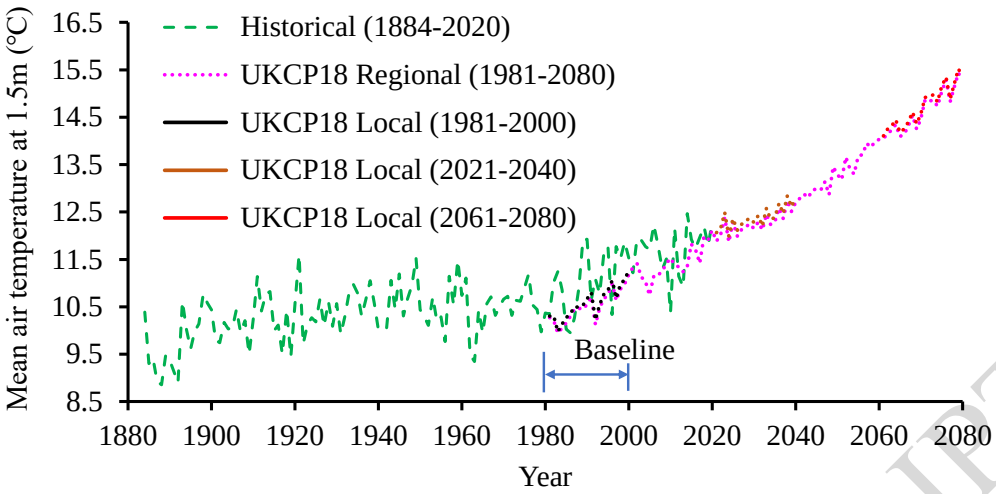

Figure 1 Annual average mean air temperature at 1.5m (°C) from the historical weather record (1884-2020) and UKCP18 projections (1981-2080, average of 12 PPEs) for Heathrow

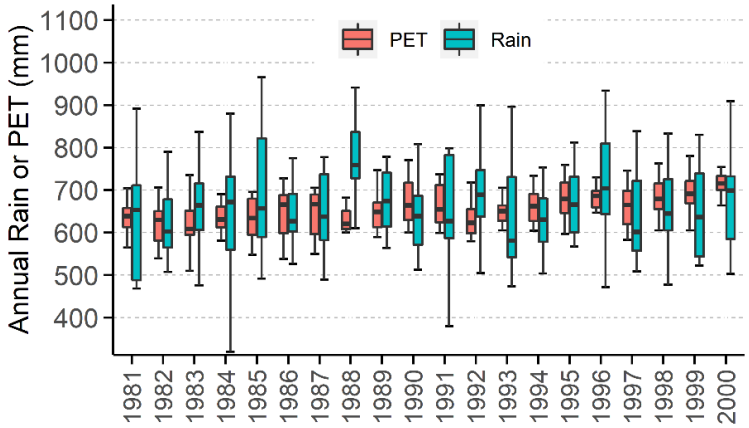

(a) 1981 – 2000

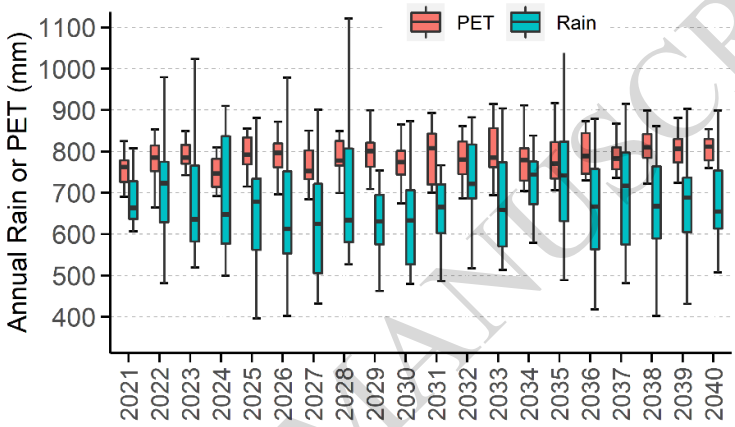

(b) 2021 – 2040

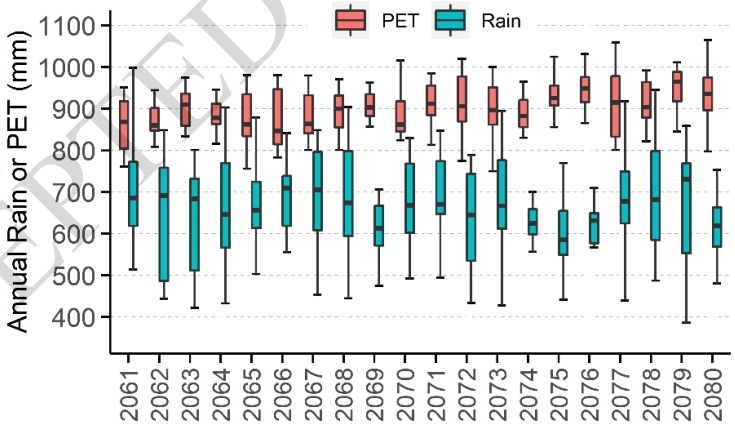

(c) 2061 – 2080

Figure 2 Annual rainfall and potential evapotranspiration (PET) from UKCP18 local projections (1981-2000, 2021-2040, 2061-2080) for London Heathrow (each boxplot shows the minimum, 25th percentile, median, 75th percentile and maximum values of the projections)

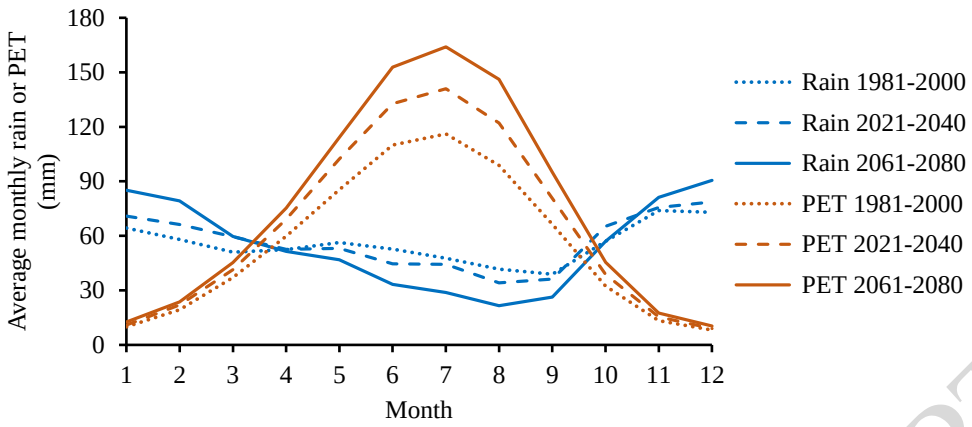

Figure 3 Average monthly rainfall and PET from UKCP18 local projections for London Heathrow (the values shown are average of the 12 PPEs)

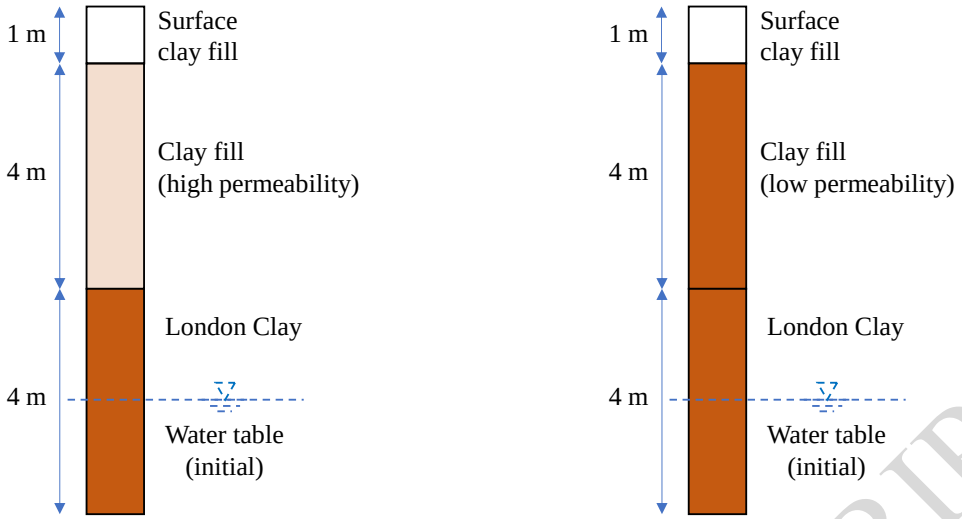

(a) High permeability (HP) (b) Low permeability (LP)

Figure 4 Representative one-dimensional models with high and low permeability clay fill (adapted from Briggs et al. 2013)

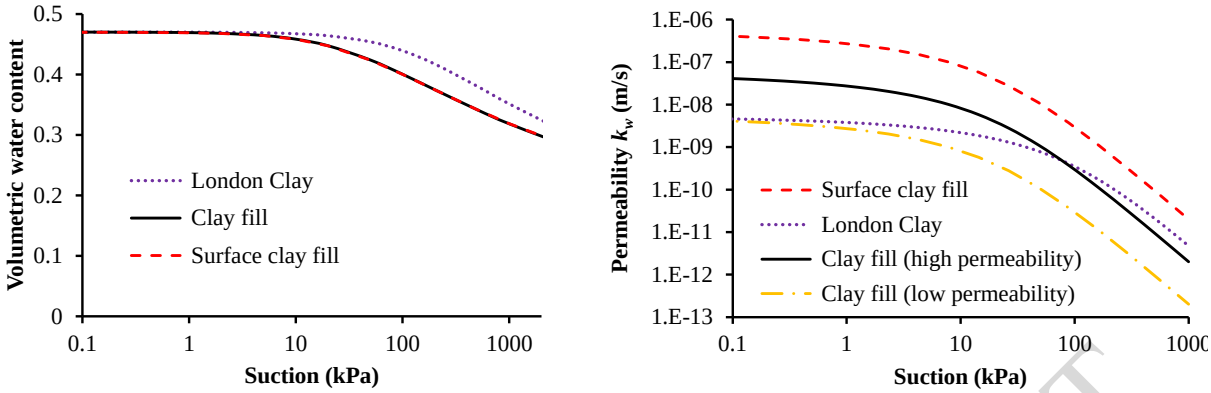

(a) Soil-water retention curve (SWRC) (b) Permeability function

Figure 5 Hydrological properties of the soils (adapted from Briggs et al. 2013)

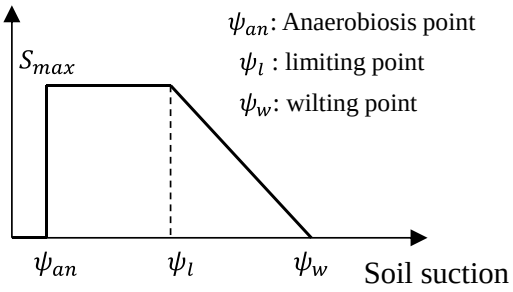

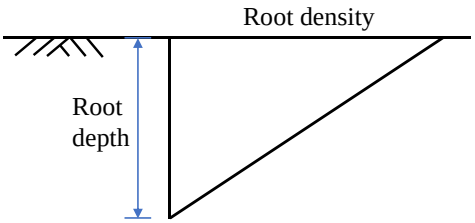

(a) Rate of root water uptake & soil suction (b) Root density distribution

Figure 6 Variation in key vegetation parameters

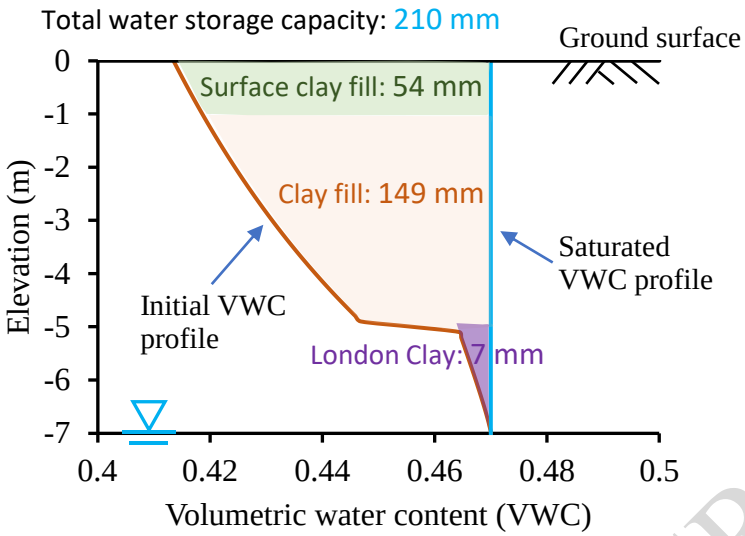

Figure 7 Water storage capacity of the ground model (relative to initial condition $t = 0$)

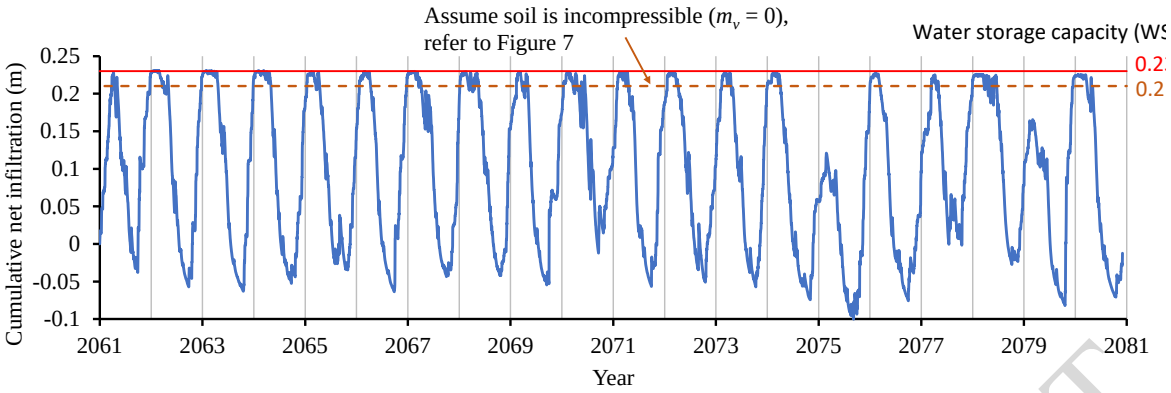

(a) Cumulative net infiltration (defined by Eq. 3b)

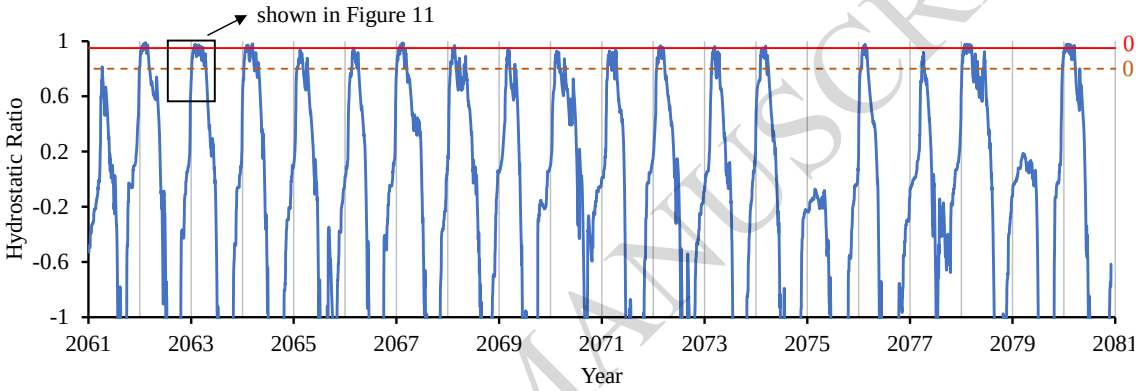

(b) Hydrostatic ratio (defined by Eq. 5)

Figure 8 Use of cumulative net infiltration, water storage capacity (WSC) and hydrostatic ratio to interpret the pore-water pressure (PWP) conditions (HP model with grass cover, climate data from PPE member 1113)

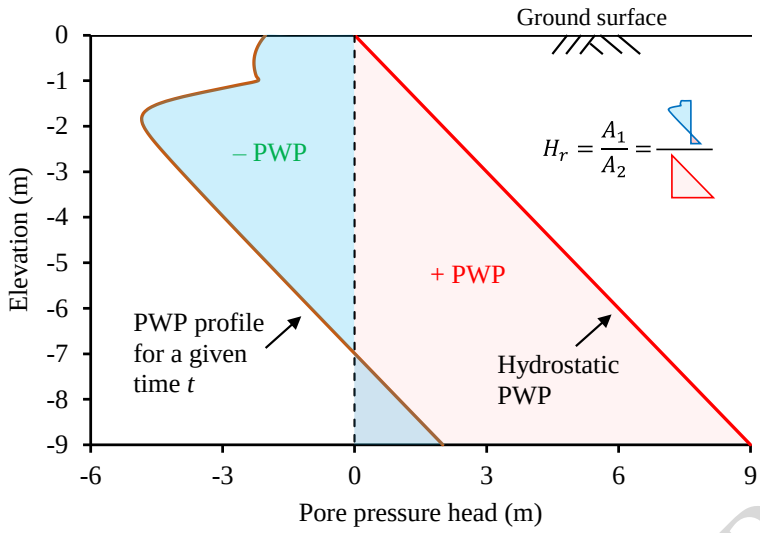

Figure 9 Definition of hydrostatic ratio H_r (calculated as the ratio of the areas enclosed by the PWP profiles and H_r can be negative)

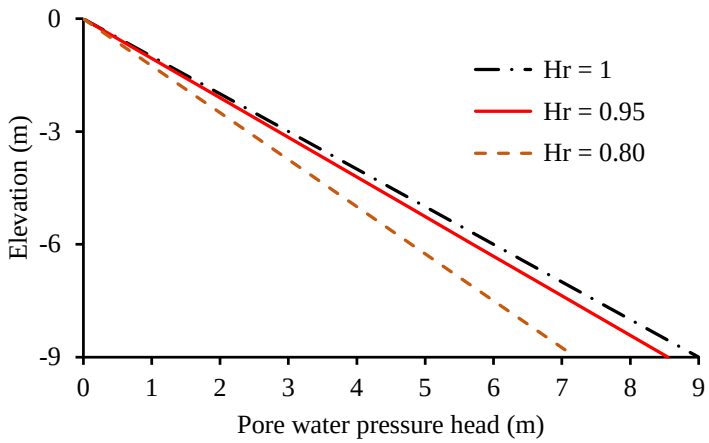

Figure 10 Illustration of pore-water pressure profiles for hydrostatic ratio (H_r) thresholds

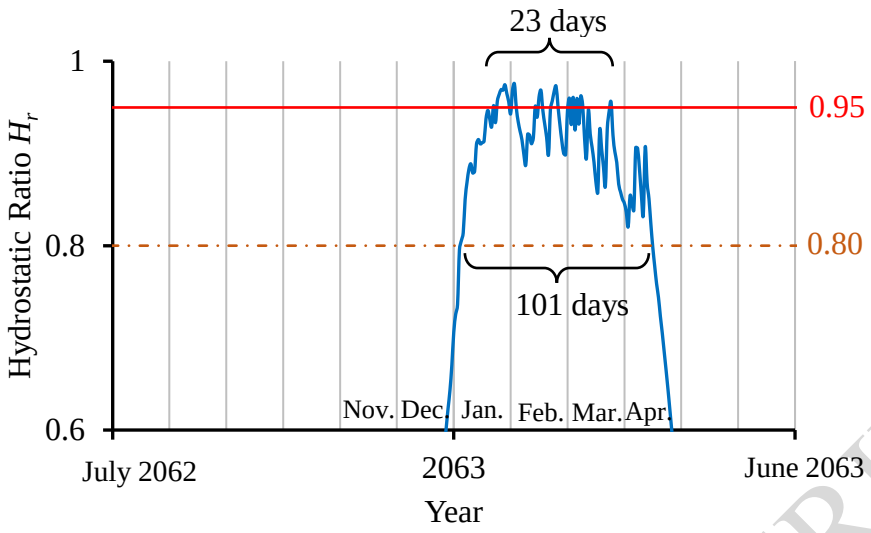

Figure 11 Determination of the number of wet days – an example (HP model with grass cover, climate data from PPE member 1113)

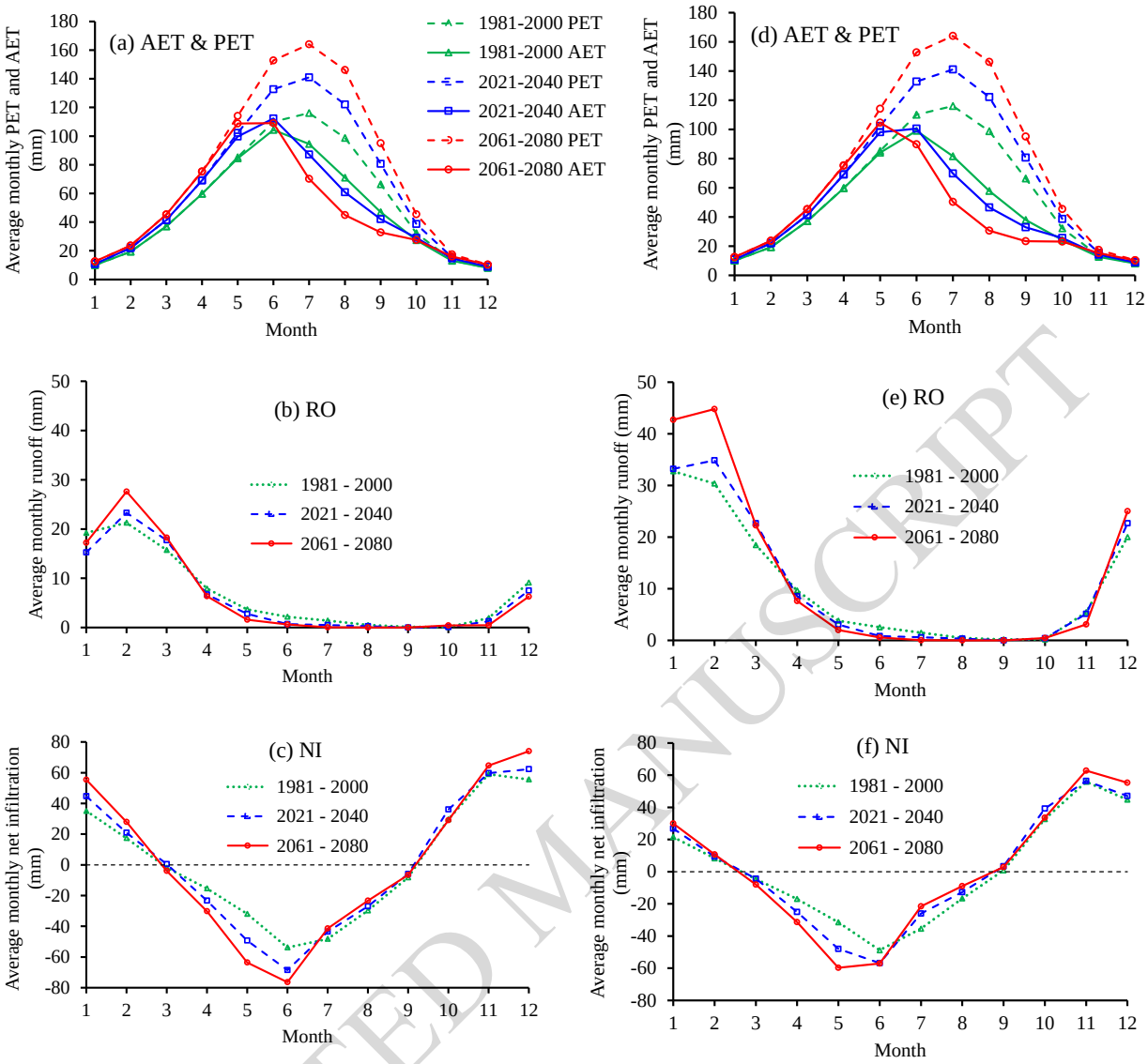

Figure 12 Water balance: (a-c) HP model with grass cover; and (d-f) LP model with grass cover (the values shown are average outputs from the 12 simulations)

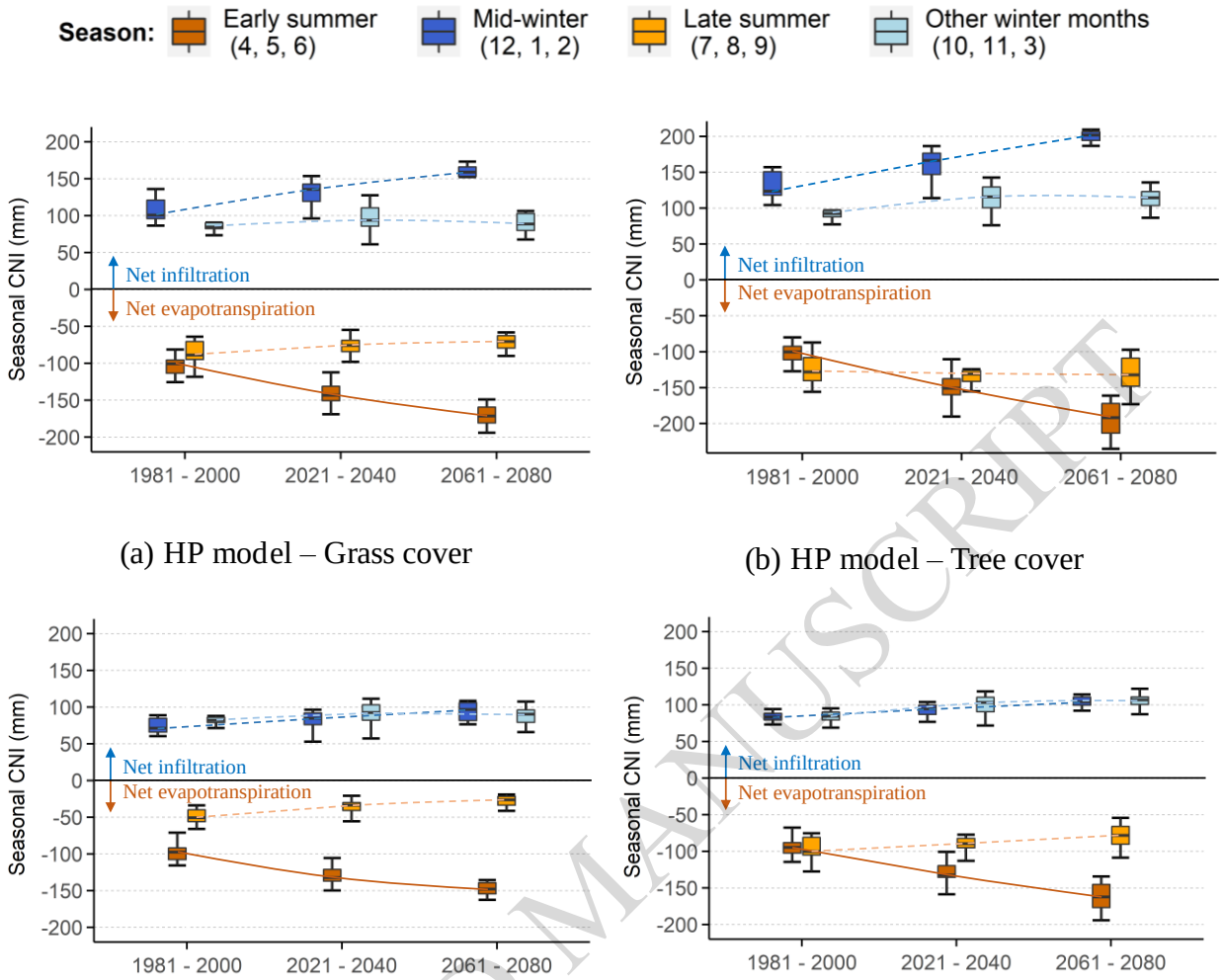

(a) HP model – Grass cover

(b) HP model – Tree cover

(c) LP model – Grass cover

(d) LP model – Tree cover

Figure 13 Change of seasonal cumulative net infiltration (CNI) with time (shown as boxplots representing 12 simulations)

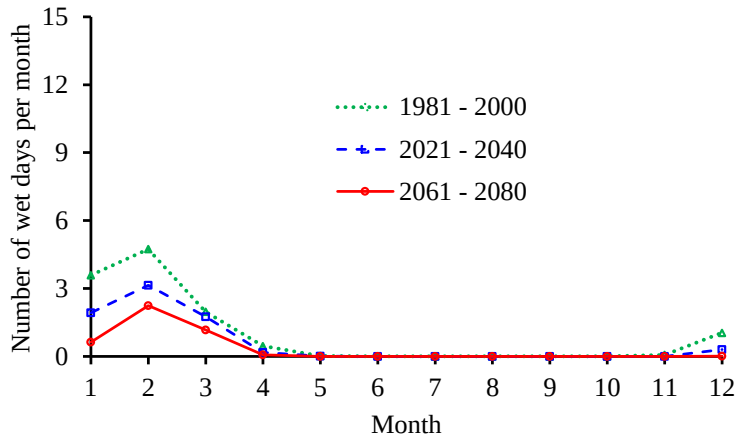

(a) Wet day criteria: $H_r \geq 0.95$

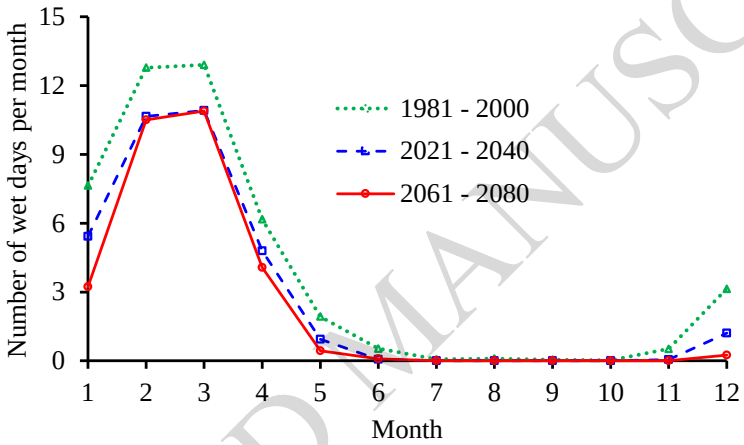

(b) Wet day criteria: $H_r \geq 0.80$

Figure 14 Average number of wet days per month for HP model with grass cover (the values shown are average outputs from 12 simulations)

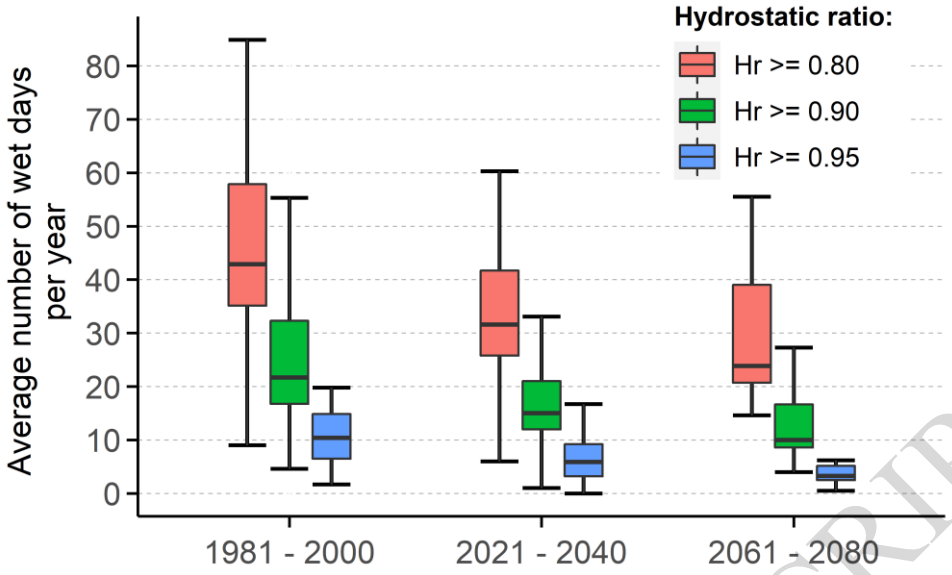

Figure 15 Average number of wet days per year from 12 simulations for HP model with grass cover

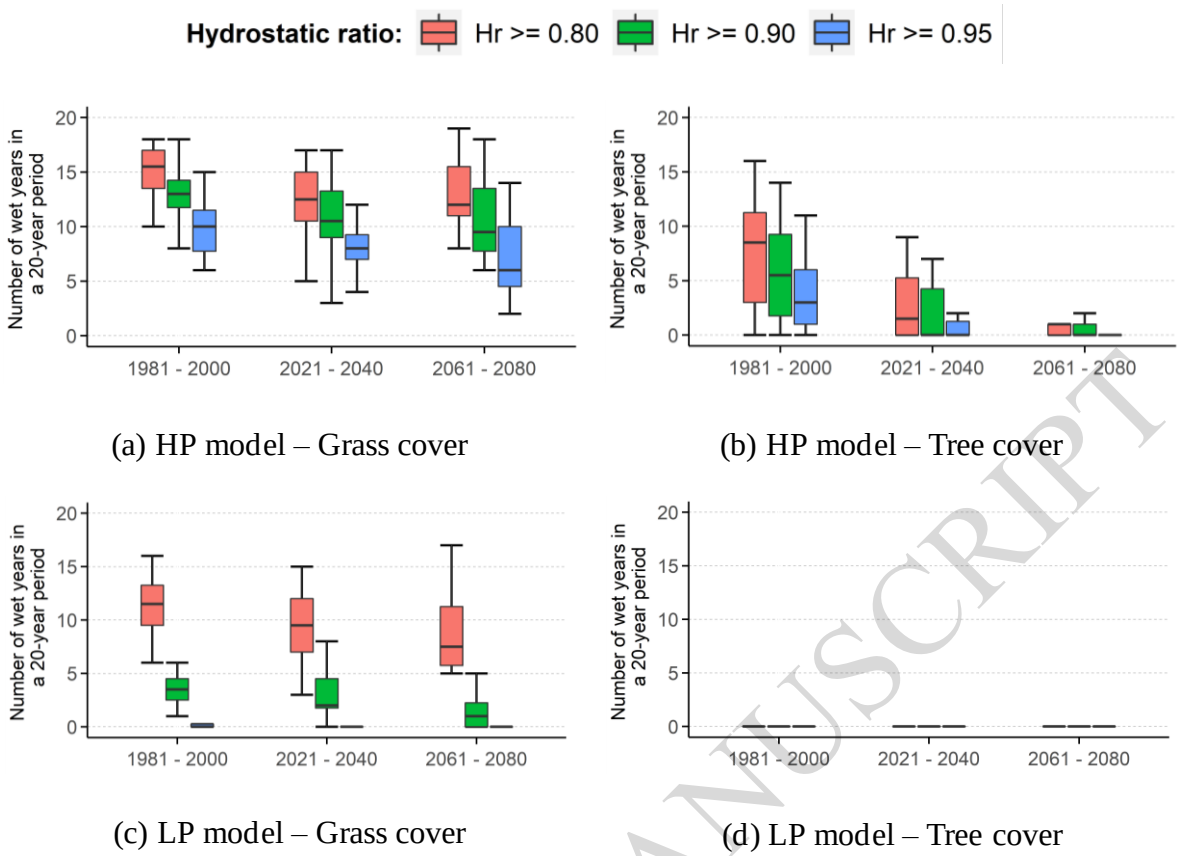

(a) HP model – Grass cover

(b) HP model – Tree cover

(c) LP model – Grass cover

(d) LP model – Tree cover

Figure 16 Number of wet years in a 20-year period in 1981-2000, 2021-2040 and 2061-2080 from 12 simulations

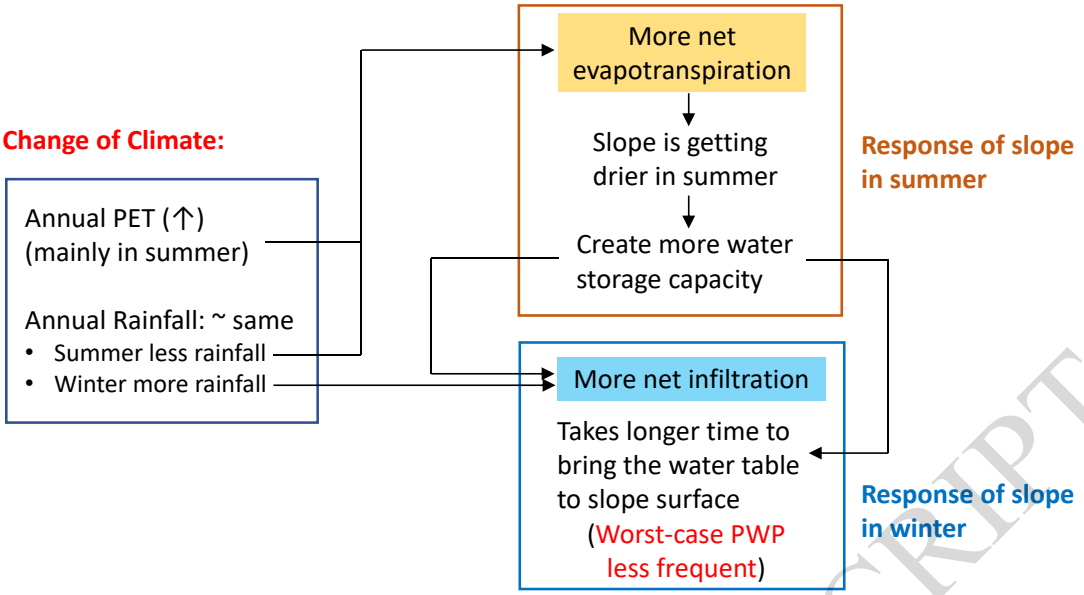

Figure 17 Change of climate and slope response in summer and winter

Table 1 Summary of numerical studies on effects of climate change on geostructures

References	Site location	Geo-structure	Climate data			Length of simulation	Modelling approach
			Historical (baseline)	Future (projected)	Modelling of climate change		
Vahedifard et al. (2017)	Seattle, US	MSE Wall	1950 – 1999	20 CMIP5 models for RCP8.5 and the period 2050 – 2099	1-day and 7-day extreme precipitations (95th upper percentile).	8 days for baseline, and 8 days for the projected. In total: 16 days	2D coupled seepage-stability analysis
Robinson et al. (2017)	Seattle, US	Natural slope	1950 – 1999	20 CMIP5 models for RCP8.5 and the period 2050 – 2099	7-day extreme precipitation (95th upper percentile)	15 days for baseline, and 15 days for the projected. In total: 30 days	2D coupled seepage-stability analysis
Pk et al. (2021)	Toronto, Canada	Highway embankment	1981 – 2010	12 models of various sources for 2011 – 2100	(1) Long-term daily precipitation and evaporation (2 subset periods); (2) 1-hour extreme precipitation.	30 years for baseline, and 60 years for the projected. In total: 90 years	2D seepage-stability analysis
Lieber et al. (2022)	Quebec, Canada	Tailings cover	2015 – 2018	18 CMIP5 and CORDEX models for RCP4.5 and RCP8.5 and the period 2020 – 2100	(1) 2 month drought; (2) Driest year; (3) 80 Year. Out of 18 climate models, three were selected.	4 years for baseline, and 243 years for the projected. In total: 247 years	1D seepage analysis (for both water and air flow)
Collison et al. (2000)	Kent, UK	Natural slope	1960 – 1990	Downscaled GCM (CCIRG91) for 1990-2079	Long-term daily precipitation and evapotranspiration	30 years for baseline, and 90 years for the projected. In total: 120 years	1D seepage-stability analysis
Dixon and Brook (2007)	Derbyshire, UK	Natural slope	1960 – 1990	UKCIP02 for medium-high scenario and 2080s	Long-term average of monthly precipitations	–	Statistical rainfall threshold analysis
Rouainia et al. (2009)	Newbury, UK	Railway embankment	UKCIP02 for 2003 scenario	UKCIP02 high emission for a 2080 scenario	Long-term daily precipitation and evapotranspiration	20 years for baseline, and 20 years for the projected. In total: 40 years	2D seepage-stability analysis
Clarke and Smethurst (2010)	London, Hemsby, Ringway, Yeovilton, UK	Engineered clay slopes	1961 – 2005 for London; 1961 – 1990 for the others.	UKCIP02 for all emission scenarios from low to high, and for 2011-2100.	Long-term daily precipitation and evapotranspiration	Baseline: 45 years for London, and 30 years for the other sites; Projected: 90 years for each site. In total: 485 years	1D soil-water balance model
Booth (2014)	Newbury, UK	Highway cutting	UKCP09 control period (1961 – 1990)	UKCP09 weather generator for high emissions and 2040-2069	Long-term daily precipitation and evapotranspiration	100 model runs, and for each 1 year was selected for baseline and the projected. In total: 200 years.	2D seepage analyses
Rouainia et al. (2020)	Newbury, UK	Highway cutting	UKCP09 control period (1961 – 1995)	UKCP09 weather generator for high emissions and 2000 – 2100	Long-term daily precipitation and evapotranspiration	100 years for the baseline, and 100 years for the projected. In total: 200 years.	2D coupled seepage-stability analysis

Guo (2021)	Essex, UK	Railway & flood embankment	1971-2000, 2007-2020	UKCP18 regional projection (RCP 8.5) for the period 2021-2080	Long-term monthly precipitation and evapotranspiration	45 years for baseline, and 60 years for the projected. In total: 105 years	2D coupled seepage-stability analysis

Table 2 Summary of soil properties used in the finite element model (adapted from Briggs et al. 2016)

	SWRC parameters (Van Genuchten, 1980)				Saturated permeability	Compressibility coefficient
	a (kPa)	m	n	θ_s	k_s (m/s)	m_v (kPa^{-1})
Surface clay fill	30.3	0.13	1.15	0.47	5×10^{-7}	5×10^{-5}
Clay fill (high permeability)	30.3	0.13	1.15	0.47	5×10^{-8}	5×10^{-5}
Clay fill (low permeability)	30.3	0.13	1.15	0.47	5×10^{-9}	5×10^{-5}
London Clay	125	0.15	1.18	0.47	5×10^{-9}	5×10^{-5}

Table 3 Summary of combination of factors in the finite element seepage analyses

Ground Model	Climate data	Time period	Vegetation type	Number of combinations
HP model, LP model	12 PPEs at daily resolution from UKCP18 local projections	1981-2000, 2021-2040, 2061-2080	Grass Tree	144 (= 2×12×3×2)

Table 4 Impact of climate change on annual dry (summer) and wet (winter) cycles (size of cycle is calculated as the sum of the absolute value of net flux at summer and winter; the percentages in the brackets are increments relative to 1981 – 2000)

	Average (rainfall – PET) (mm)			Average net infiltration (mm) (HP model – Grass cover)			Average net infiltration (mm) (HP model – Tree cover)		
	Summer	Winter	Size of cycle	Summer	Winter	Size of cycle	Summer	Winter	Size of cycle
1981-2000	-247	257	504	-187	194	381	-225	224	449
2021-2040	-383 (55%)	279 (8%)	662 (31%)	-218 (16%)	223 (15%)	441 (16%)	-282 (25%)	275 (23%)	557 (24%)
2061-2080	-539 (119%)	298 (16%)	837 (66%)	-242 (29%)	246 (27%)	488 (28%)	-325 (44%)	313 (40%)	638 (42%)

	Average net infiltration (mm) (LP model – Grass cover)			Average net infiltration (mm) (LP model – Tree cover)		
	Summer	Winter	Size of cycle	Summer	Winter	Size of cycle
1981-2000	-149	158	306	-192	169	361
2021-2040	-165 (11%)	174 (10%)	339 (11%)	-221 (15%)	194 (15%)	415 (15%)
2061-2080	-176 (18%)	183 (16%)	359 (17%)	-241 (25%)	211 (25%)	452 (25%)